The anisotropic electron - positron momentum distribution in diamond

1997 J. Phys.: Condens. Matter 9 6323

(http://iopscience.iop.org/0953-8984/9/29/017)

J. Phys.: Condens. Matter **9** (1997) 6323–6333. Printed in the UK PII: S0953-8984(97)81688-8

The anisotropic electron–positron momentum distribution in diamond

R W N Nilen†, S H Connell†, D T Britton‡, C G Fischer†, E J Sendezera§, P Schaaff†‖, W G Schmidt¶, J P F Sellschop† and W S Verwoerd+

† Schonland Research Centre for Nuclear Sciences, University of the Witwatersrand, PO Wits, 2050, Johannesburg, South Africa

‡ Physics Department, University of Cape Town, Rondebosch, 7700, South Africa

§ Physics Department, University of Zululand, P Bag X1001, KwaDlangezwa, 3886, South Africa

‖ Institut für Kern- und Strahlenphysik der Universität Bonn, Nussallee 14–16, 53115 Bonn, Germany

¶ Friedrich-Schiller-Universität Jena, Institut für Festkörpertheorie und Theoretische Optik, Max-Wien-Platz 1, 07743 Jena, Germany

+ Physics Department, University of South Africa, PO Box 392, Pretoria 0001, South Africa

Received 7 February 1997, in final form 6 May 1997

Abstract. We have performed a high-resolution, high-sensitivity study of the electron–positron momentum distribution in diamond, using the two-detector coincidence Doppler broadening technique of positron annihilation spectroscopy. The measurements were carried out with the ⟨100⟩, ⟨110⟩, and ⟨111⟩ axes each separately aligned collinearly with the detectors so that the anisotropy of the momentum distribution could be mapped out. Small differences in the momentum profiles were enhanced with difference spectra, and compare well with results of a density-functional theory calculation of the electron–positron momentum distribution in the diamond lattice. There has been much debate regarding previously unexplained anomalies in the annihilation characteristics of the bulk positron configuration in diamond. These new results strongly support a model describing the bulk positron as delocalized and inhomogeneous, but with sufficient amplitude at the intra-bond region such that the annihilation characteristics are determined by the bond electron density and momentum distribution.

1. Introduction

Thermalized positrons in solids annihilate with core and valence electrons after the formation of well defined configurations which represent delocalized or trapped positron states [1]. Two configurations are usually identified for the positron in the diamond lattice. The first has a large electron–positron density overlap, resulting in a short lifetime (∼114 ps), and accounts for as much as 80–100% of the positrons implanted into the lattice [2–4]. Age–momentum correlation measurements have identified this short-lifetime configuration with an extremely broad momentum distribution (approximately 3.5 keV/c FWHM) [2]. The combination of these characteristics has resulted in much debate regarding the electron–positron configuration responsible for this state. Neither positronium formation nor annihilation in the interstitial regions of the lattice can account simultaneously for the high initial population, short-lifetime, and broad momentum distribution of the state. It

0953-8984/97/296323+11$19.50

has been proposed that annihilation from a delocalized positron state, where the electron–positron overlap distribution has a large contribution from the carbon–carbon bond region, is a plausible model for this configuration [5].

The values measured for the bulk positron lifetime in diamond published to date range from (approximately) 98 ps [4] to 120 ps [3]. It is proposed that this spread is the result of contributions from defect-related positron configurations which have lifetimes too close to the bulk lifetime to be fully resolved. This has been demonstrated in age–momentum correlation measurements on industrial-grade diamond [6]. Only one lifetime component with a lifetime close to the theoretical value reported in this paper (section 5) was observed in an especially defect-free sample [4]. Similarly, positronium formation in the diamond lattice has only been observed in defect-related configurations, such as in the grain boundaries between the crystallites of natural diamond [7].

The second configuration has a longer lifetime and smaller momentum spread (both sample dependent), and accounts for the remaining implanted positrons. This state is linked to positron trapping and annihilation at lattice defects. The transition from the first to the second state occurs at a rate of approximately 10^9 s^{-1} at room temperature, and is well described by the two-state trapping model [8].

The anisotropy of the electron–positron momentum distribution in diamond has been theoretically investigated with two-component density-functional theory, where the momentum distributions of diamond, Si, and Ge were compared [9]. The authors concluded that the difference in the low-momentum region of diamond is due to the small lattice constant and weaker electron–positron correlation effects. Experimentally, orientation-dependent single-detector, one-detector Doppler broadening [5], as well as two-dimensional (2D) ACAR (angular correlation of annihilation radiation) [9, 10] studies have been performed.

The current paper reports on two-detector coincidence Doppler broadening measurements carried out on a synthetic diamond sample. The measurements were performed at different crystallographic orientations to study the anisotropy of the electron–positron momentum distribution. The main advantage of the two-detector technique introduced by Lynn *et al* [11] over the conventional one-detector technique is that peak-to-background ratios of better than 10^5:1 are possible. Thus high-momentum components can be efficiently observed in the energy spectra. In addition, the energy resolution of the spectrometer can be improved by a factor of $\sqrt{2}$, and the binding energy of the electron–positron system and the host can be measured. As a result of the increased resolution and sensitivity of the technique, the experiments represent a dramatic enhancement over the previous one-detector measurements (reference [5]) of the anisotropic electron–positron momentum distribution in diamond.

2. Two-detector coincidence Doppler broadening spectroscopy

The Doppler broadening technique of positron annihilation spectroscopy allows the measurement of the longitudinal projection of the momentum distribution of annihilating electron–positron pairs in solid-state studies. The annihilation photons have energies given by

$$E_1 = E_0 - E_b/2 + \Delta E + \delta_1 \tag{1}$$

$$E_2 = E_0 - E_b/2 - \Delta E + \delta_2 \tag{2}$$

where E_b is the binding energy of the electron–positron system and the host, E_0 the rest mass of the electron (511 keV), and $\delta_{1,2}$ the individual errors due to the detector resolutions.

The Doppler shifts (ΔE) on the annihilation quanta provide a measure of the longitudinal projection of the momentum distribution (P_L) of the annihilating pair according to

$$\Delta E = cP_L/2 \tag{3}$$

where c is the speed of light. From (1) and (2), the sum and difference of the two γ-ray energies are given by

$$E_1 + E_2 = 2E_0 - E_b + (\delta_1 + \delta_2) \tag{4}$$

$$E_1 - E_2 = 2\,\Delta E + (\delta_1 - \delta_2). \tag{5}$$

The energy sum (4) thus contains information regarding the binding energy of the electron–positron system and the host, and the Doppler broadening is doubled in the energy difference (5). In such a measurement, the energy of the first photon is plotted against the energy of the second in a two-dimensional histogram. As indicated in figure 1 and equation (5), the positive-gradient diagonals of this histogram represent lines of constant energy difference. Thus plotting the data for $E_1 - E_2$ on the locus $E_1 + E_2$ displays the momentum distribution of the annihilating pair in the state characterized by a binding energy E_b. Due to energy resolution considerations, and to improve the statistics, we projected the $E_1 - E_2$ data onto the locus for a centred band of 1.6 keV about the line, as indicated by the dashed lines in figure 1.

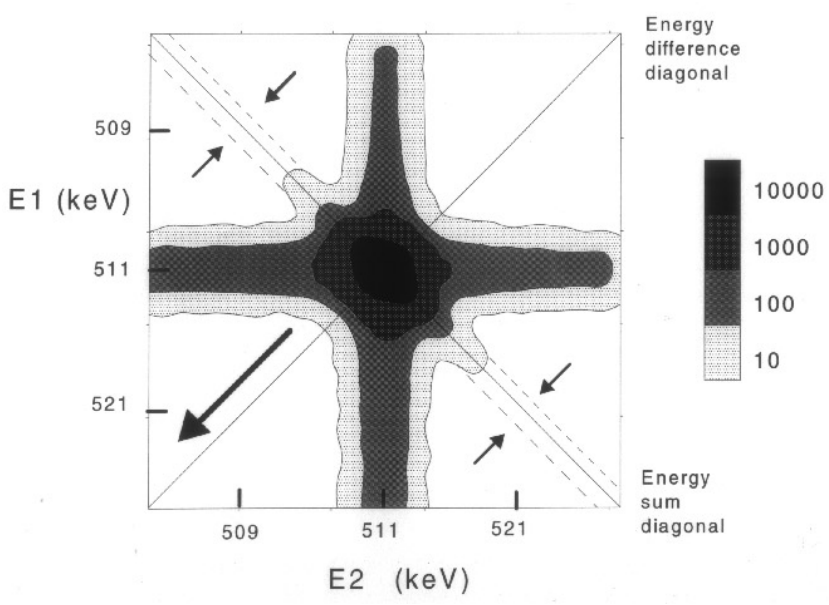

Figure 1. The two-detector coincidence measurement of both annihilation quanta with a double-detector Doppler-broadening spectrometer. The contour levels are logarithmic, and scale from 1 (white) to 10^5 (black), and the large arrow indicates the direction of increasing binding energy. The dashed lines represent the projection bandwidth for the extraction of the momentum profile (see the text).

The individual detector resolutions $\delta_{1,2}$ are not correlated, and therefore do not add linearly. An overall improvement in the energy resolution of the spectrometer by a factor of $\sqrt{2}$ is thus achieved for two detectors with the same resolution [12]. As can be seen in figure 1, the high-momentum tails of the extracted projection are free of Compton

scattered photons, and peak-to-background ratios better than 10^5:1 are attainable. The reduced background and improved energy resolution of this technique permit the efficient measurement of the core-electron contribution to electron–positron momentum distributions in condensed matter. The slight asymmetry about the energy sum diagonal is a result of the binding energy of the electron–positron pair and the host. The spectrometer design is shown in figure 2.

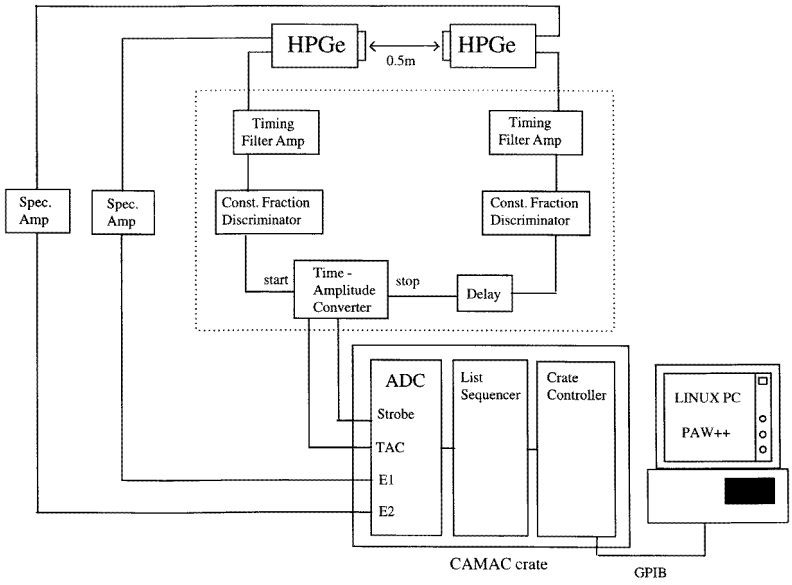

Figure 2. A high-resolution spectrometer for source-based electron–positron momentum distribution measurements.

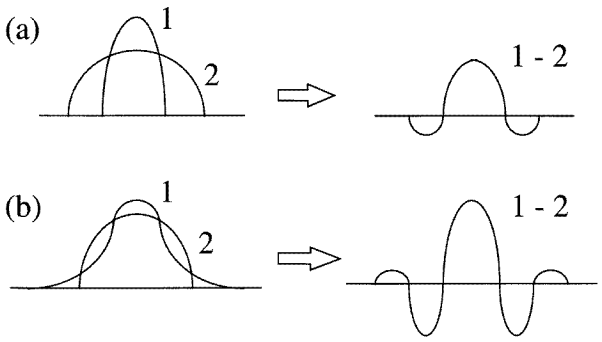

Figure 3. Difference spectra emphasize small changes in the low-energy regions of the momentum profiles.

High-purity germanium detectors (HPGe) are used to measure the energy of the annihilation quanta. The time interval between the detection of one γ-quantum and the next is recorded with a time-to-amplitude converter in a separate fast-timing circuit (inside the dotted box in figure 2) to determine whether they were detected within a certain coincidence window, indicating a true annihilation event. The width of the time coincidence window

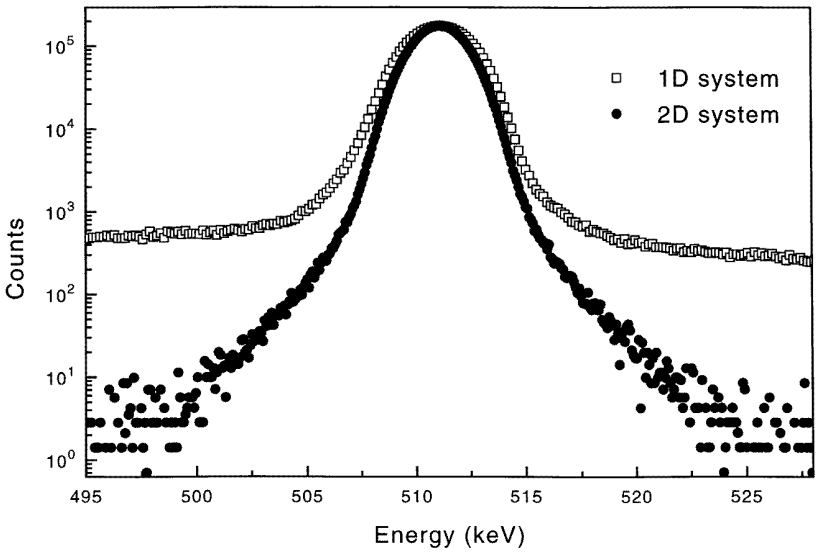

Figure 4. The improved energy resolution and reduced background of a two-detector measurement allow the efficient observation of core-electron contributions to the electron–positron momentum distribution in condensed matter.

(typically 5 ns) and the energy gating were software controlled in the computerized data acquisition system (DAS). The DAS comprised a CAMAC-controlled analogue-to-digital converter (ADC) coupled to a list sequencer and crate controller. Communication between the DAS software (PAW++ [13]) and the buffered events from the CAMAC crate was via a separate experiment control task using shared memory. The design and operation of similar spectrometers can be found in references [14, 15]. The one-detector Doppler broadening technique is usually only amenable to extraction of phenomenological parameters describing gross features of the momentum distribution, such as the so-called *S*-parameter. The *S*-parameter is defined as the ratio of the central region of the photopeak to the total peak area, and is thus inversely related to the Doppler broadening. In contrast, the resolution and sensitivity of two-detector coincidence Doppler broadening measurements is sufficient for the longitudinal projection of the momentum distribution to be studied and compared to theory. Small changes in the low-energy region of the distinct momentum profiles can be amplified by taking appropriate difference spectra [16]. Figure 3 is a schematic illustration of the process for two simple cases, and aids in the interpretation of the resulting spectra.

As the momentum profiles are symmetric about 511 keV, they are usually folded about 511 keV for improved statistics. This is the case for the results presented in figure 5—see later.

3. Experiment

As is common in source-based positron annihilation spectroscopy experiments, the sample was prepared in a sandwich arrangement containing a 15 μCi ^{22}Na (β^+-emitter) deposit. Further details regarding the preparation procedure developed for diamond samples can be found in reference [5]. The synthetic diamond sample was optically characterized at room temperature, and a 214 ppm concentration of P1 centres (single-substitutional nitrogen

atoms) was observed in the infra-red absorption spectrum. The stone was thus classified as type Ib. The dimensions of the sample ($4 \times 4 \times 3$ mm^3) ensured that all emitted positrons annihilated in the diamond bulk.

The detectors were placed 25 cm (see figure 2) from the sample, giving the spectrometer an angular resolution of roughly 4°. The singles event rate in each detector was roughly 420 s^{-1}, corresponding to an event rate of approximately 100 s^{-1} in the two-dimensional spectra. The individual resolutions of the detectors were measured using the 477 keV line of ^{7}Be to be 1.1 keV, yielding an effective energy resolution of approximately 850 eV (FWHM) at 511 keV for the spectrometer. Figure 4 shows the clear advantages of a two-detector measurement over a conventional one-detector measurement.

All of the measurements were performed at room temperature in the atmosphere. X-ray Laue photographs were used to orientate the sample, and data were collected with the ⟨100⟩ axis aligned collinearly with the detectors. The measurements were then repeated for the ⟨110⟩ and ⟨111⟩ axes. Each two-dimensional spectrum contained approximately 6×10^6 events, and took roughly twenty hours to collect. As the spectra were collected in list mode, event-by-event playback was possible, and the centroid positions of the 511 keV and 1275 keV lines in the single-detector spectra could be monitored over time to check the stability of the spectrometer. There were no stability problems during the course of the experiment.

4. Theory

A theoretical calculation of the positron lifetime and the electron–positron momentum distribution in perfect diamond was carried out using an *ab initio* pseudopotential approach based on two-component density-functional theory (DFT). For a delocalized positron the positron density at every point in the infinite lattice is vanishingly small, and therefore cannot influence the electronic structure. The two-component DFT thus simplifies to one-component DFT in this case. Details of the calculation are given in references [5, 17] and a recent review of theoretical calculations in positron spectroscopy can be found in reference [18]. Due to core repulsion, positron annihilation with core electrons is expected to be minimal (less than 2% [19]). Core electrons were thus ignored in this calculation.

For the lifetime calculation, the electron–positron correlation was modelled with a local density approximation using the parametrization of Boronski and Nieminen [20], scaled to take into account the reduced screening due to the presence of the band gap in diamond. The positron lifetime is the inverse of the annihilation rate, given by

$$\lambda = \pi r_0^2 c \int \mathrm{d}\boldsymbol{r}\; n_+(\boldsymbol{r}) n_-(\boldsymbol{r}) g(0; n_+, n_-) \tag{6}$$

where $g(0; n_+, n_-)$ is the electron–positron pair correlation function for positron density n_+ and electron density n_-, r_0 is the classical electron radius, and c is the speed of light. The electron–positron density overlap distribution, a calculation of the integral of equation (6), represents a mapping of the electron–positron annihilation probability density. Calculated results are shown in figure 6—see later—and are discussed in the next section.

The contribution of the delocalized, thermalized positron to the momentum of the annihilating pair is very small. Accordingly, an independent-particle model (IPM) approach was used to calculate the electron–positron momentum distribution in perfect diamond, given by

$$\rho(\boldsymbol{P}) = 2 \sum_{n,\boldsymbol{k}} f(n, \boldsymbol{k}) \left| \int_\Omega \mathrm{d}r\; \mathrm{e}^{-\mathrm{i}\boldsymbol{P}\cdot\boldsymbol{r}} \psi^+(\boldsymbol{r}) \psi^-_{n,\boldsymbol{k}}(\boldsymbol{r}) \right|^2 \delta_{\boldsymbol{P},\boldsymbol{k}+\boldsymbol{G}} \tag{7}$$

where $f(n, \boldsymbol{k})$ is the Fermi function, $\psi^{-}_{n,\boldsymbol{k}}(\boldsymbol{r})$ is the electron Bloch state with band index n and wave vector $\boldsymbol{k}$, Ω is the volume of the primitive cell, and $\boldsymbol{G}$ denotes a reciprocal-lattice vector. Projections of this momentum distribution onto the $\langle 100\rangle$, $\langle 110\rangle$, and $\langle 111\rangle$ axes were then taken to allow a direct comparison with experiment. These comparisons are included in figure 5 as difference spectra, and are discussed below.

5. Results and discussion

Difference spectra, both theoretical and experimental, have been generated to allow a detailed investigation of the low-energy region of the electron–positron momentum distribution in diamond. All of the spectra, both experimental and theoretical, were normalized to unity before subtraction, and the momentum profiles have been folded about 511 keV for improved statistics. The results are plotted in figure 5.

Figures 5(a) and 5(b) exhibit a character similar to that presented schematically in figure 3, case (b). Specifically, they indicate that the momentum distribution projected onto the $\langle 111\rangle$ axis resembles profile 2 in figure 3(b) with respect to both the $\langle 100\rangle$ and $\langle 110\rangle$ axes, i.e. is broader in the middle regions (from roughly 511.5 keV to 513 keV), but without the very high-momentum component tails of the $\langle 100\rangle$ and $\langle 110\rangle$ axes above 513 keV. This agrees well with the one-detector measurement reported earlier [5], where minima in the *S*-parameter were observed for projections of the momentum distribution onto the $\langle 111\rangle$ axes.

The data presented in figure 5(c) provide the clearest example of the advantages that a two-detector coincidence measurement has over a one-detector measurement. In the *S*-parameter analysis of the data taken in the one-detector measurement, the projections of the momentum distribution onto the $\langle 100\rangle$ and $\langle 110\rangle$ axes yielded almost identical *S*-parameters. However, the two-detector investigation presented in figure 5(c) reveals clear differences in the momentum profiles not picked up by the *S*-parameter treatment. The presence of two maxima at approximately 510 keV and 512 keV in this difference spectrum reflects the anisotropic nature of the electron–positron momentum distribution in the diamond lattice.

Included in figure 5 are the corresponding difference spectra obtained from the theoretical calculation of the electron–positron momentum distribution in diamond. The qualitative agreement is fair, particularly in figure 5(c) where the double peak in the unfolded momentum profile difference spectrum is successfully predicted. However, quantitatively the curves differ significantly. After convoluting the theoretical curves with a Gaussian model of the energy resolution of the spectrometer, they show a variation approximately 1.5 times greater than that of the experimental curves. This discrepancy is attributed partly to the fact that the experiment was performed at room temperature, whereas temperature effects were ignored in the theoretical calculation. Temperature is expected to broaden the momentum profiles, and thus decrease the magnitude of any variations. Dannefaer *et al* [21] recently demonstrated this effect in Doppler broadening studies of several diamond-like semiconductors. They observed an increase in the *S*-parameter by as much as 0.3% from 100 to 300 K in one-detector measurements on GaAs. This broadening effect has also been observed for the polarization-dependent reflectance anisotropy of semiconductor surfaces [22], where measurements at liquid helium temperature showed a variation roughly four times greater than that of measurements performed at room temperature. The presence of defects in the diamond lattice also contributes significantly to the quantitative discrepancy. Subsequent lifetime measurements on the sample revealed a 14(1)% trapped positron intensity. The trapped positron contribution to the electron–positron momentum distribution cannot be reliably extracted, and so will significantly reduce any observed anisotropy. In

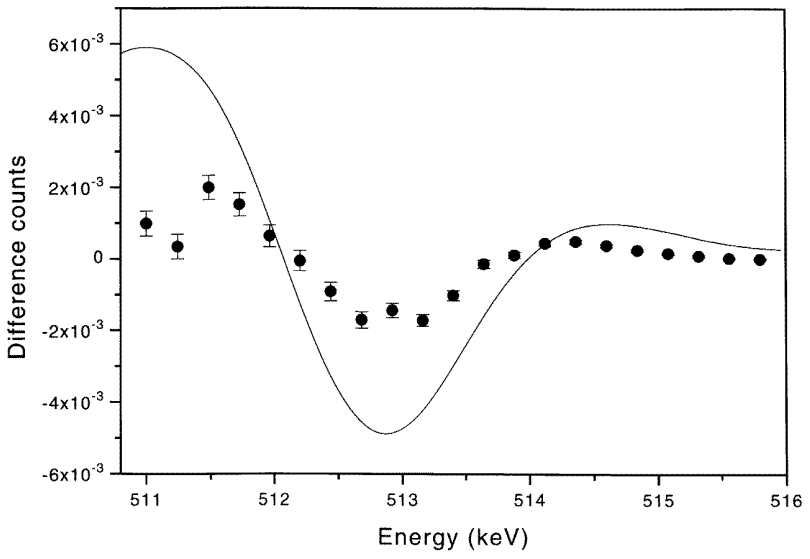

(a)

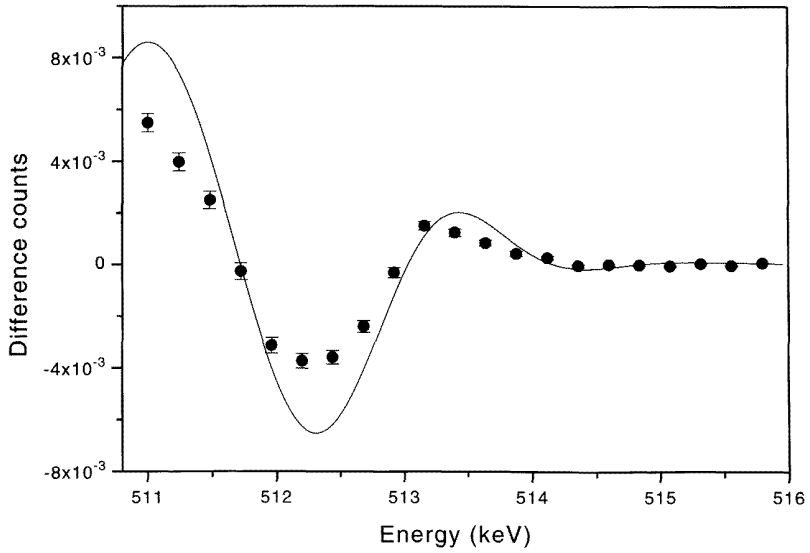

(b)

Figure 5. Difference spectra enhance subtle anisotropies in the electron–positron momentum distributions for the three major crystallographic orientations of diamond. The predictions of the density-functional theory calculation of the difference spectra have been included on the same scale to highlight the good qualitative agreement. The quantitative discrepancies are discussed in the text. (a) $\langle 100\rangle - \langle 111\rangle$; (b) $\langle 110\rangle - \langle 111\rangle$; (c) $\langle 100\rangle - \langle 110\rangle$.

addition, the (approximately) 4° angular resolution of the spectrometer, the independent-particle model treatment of the electron–positron correlation, and the use of pseudopotentials to calculate the electron density contribute.

The calculation of the electron–positron annihilation rate (equation (6)) yielded a bulk

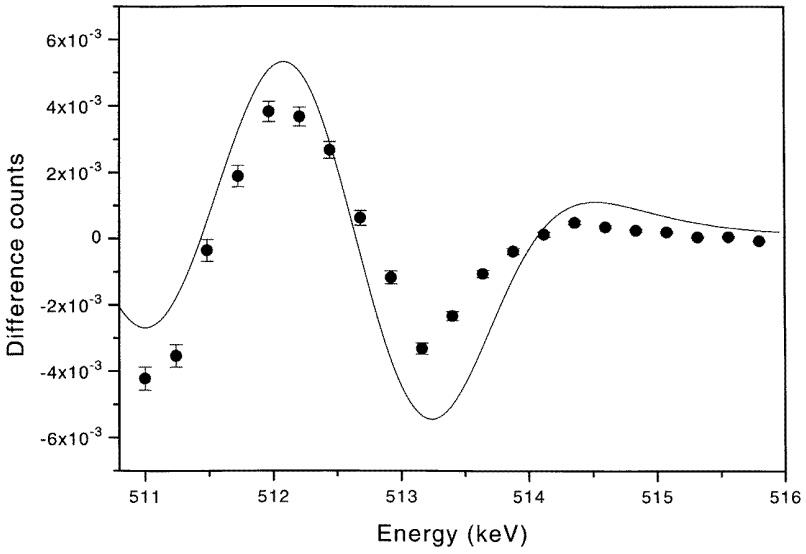

(c)

Figure 5. (Continued)

positron lifetime of 96 ps. This is in excellent agreement with the experimental results of Li *et al* [4] who recorded a bulk positron lifetime of 97.5 ± 1.5 ps for an isotopically pure synthetic diamond. Figure 6 is a plot of the calculated electron–positron density overlap distribution in the [110] plane.

This distribution assumes a maximum in the bond regions. To compare the total annihilation intensity in the bond and interstitial regions, the bond region was defined as any site with an electron density parameter $r_s < 1.34$ (atomic units). The dashed line in figure 6 indicates the chosen interface between these two regions. The total probability weights were then calculated. This rough method of calculation yielded a ratio of bond-region annihilation to interstitial region annihilation of 1:1 ($\pm 5\%$). Thus, despite repulsion due to the carbon cores, there is a high probability of annihilation in the bond region. It is suggested that this explains the broad momentum distribution observed for the short-lived positron configuration in diamond.

6. Conclusion

The two-detector coincidence Doppler broadening technique of positron annihilation spectroscopy allows a high-resolution measurement of the electron–positron momentum distribution in condensed matter. Measurements have been performed on a synthetic diamond sample as a function of crystallographic orientation, and the anisotropy of the electron–positron momentum distribution was investigated. The experimental results are in good agreement with a density-functional theory calculation of the electron–positron momentum density distribution.

It has been demonstrated that the broad momentum distribution of the bulk positron configuration in the diamond lattice can be attributed to positron annihilation with electrons in the carbon–carbon bond region. These new results indicate that although the positron density is small in the bond region, due to core repulsion, the extreme localization of the

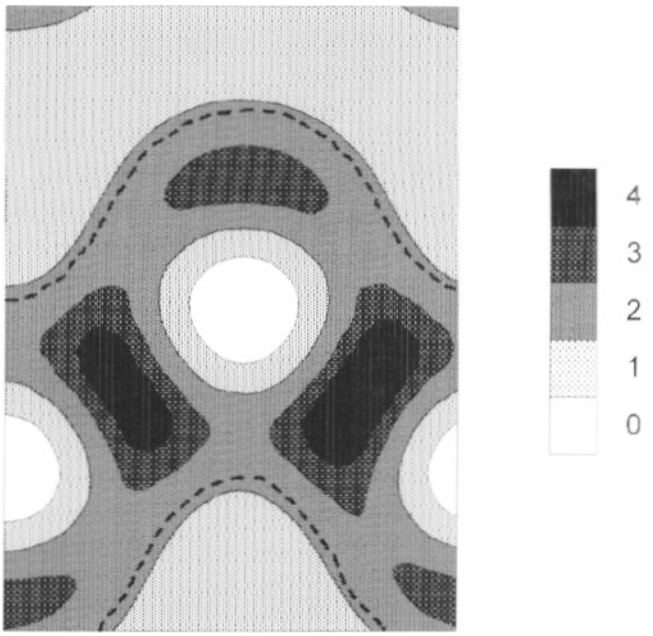

Figure 6. The overlap distribution of the electron–positron densities in a [110] plane showing the pile-up in the bond region. The contour levels scale from 0 (white) to 4 (black) in arbitrary units. The dashed line represents the bond-region/interstitial region boundary chosen for the annihilation site estimate discussed in the text.

electron density there compensates for this, such that the annihilation characteristics of the positron in bulk diamond are determined by the bond electrons. This model can therefore explain simultaneously the high initial population, short lifetime, and broad momentum distribution of the bulk positron state. In pure diamond, this should be the only state for deeply implanted positrons. The spread in the reported bulk positron lifetimes, the appearance of other lifetime components, and the observation of positronium formation in the diamond lattice are due to defect-related positron configurations.

Acknowledgment

The authors would like to thank Messrs de Beers Industrial Diamond Division (Pty) Ltd for support, in particular as regards the provision of materials.

References

[1] For an early review, see e.g.
West R N 1973 *Adv. Phys.* **22** 263
[2] Koch M, Maier K, Major J, Seeger A, Sellschop J P F, Sideras-Haddad E, Stoll H and Connell S H 1992 *Mater. Sci. Forum* **105–110** 671
[3] Dannefaer S, Mascher P and Kerr D 1992 *Diamond Relat. Mater.* **1** 407
[4] Li Y S, Berko S and Mills A P Jr 1992 *Mater. Sci. Forum* **105–110** 739
[5] Nilen R W N, Connell S H, Schmidt W G, Britton D T, Verwoerd W S, Sellschop J P F and Shrivastava S 1997 *Appl. Surf. Sci.* **116** 330
[6] Lauff U, Nilen R W N, Connell S H, Stoll H, Bharuth-Ram K, Siegle A, Schneider H, Hamart P, Wesolowski P, Sellschop J P F and Seeger A 1997 *Appl. Surf. Sci.* **116** 268

[7] Fujii S, Nishibayashi Y, Shikata S, Uedono A and Tanigawa S 1995 *J. Appl. Phys.* **78** 1510
[8] Seeger A 1973 *J. Phys. F: Met. Phys.* **3** 248
[9] Panda B K, Fung S and Beling C D 1996 *Phys. Rev.* B **53** 1251
[10] Liu W, Berko S and Mills A P Jr 1992 *Mater. Sci. Forum* **105–110** 743
[11] Lynn K G, MacDonald J R, Boie R A, Feldman L C, Gabbe J D, Robbins M F, Bonderup E and Golovchenko J 1977 *Phys. Rev. Lett.* **38** 241
[12] Britton D T, Junker W and Sperr P 1992 *Mater. Sci. Forum* **105–110** 1845
[13] *Physics Analysis Workstation* CERN Program Library Entry Q121
[14] MacDonald J R, Lynn K G, Boie R A and Robbins M F 1978 *Nucl. Instrum. Methods* **153** 189
[15] Matsui S 1992 *J. Phys. Soc. Japan* **61** 187
[16] MacKenzie I K 1983 *Positron Solid State Physics, Proc. Int. 'Enrico Fermi' School of Physics, Course LXXXIII (Varenna, 1981)* ed W Brandt and A Dupasquier (Amsterdam: North-Holland) p 659
[17] Schmidt W G and Verwoerd W S 1996 *Phys. Lett.* **222A** 275
[18] Puska M J and Nieminen R M 1994 *Rev. Mod. Phys.* **66** 841
[19] Puska M J, Makinen S, Manninen M and Nieminen R M 1989 *Phys. Rev.* B **39** 7666
[20] Boronski E and Nieminen R M 1986 *Phys. Rev.* B **34** 3820
[21] Dannefaer S, Puff W and Kerr D 1997 *Phys. Rev.* B **55** 2182
[22] Berkovits V L, Makarenko I V, Minashvili T A and Safarov V I 1985 *Solid State Commun.* **56** 449